"This is an Accepted Manuscript of an article published by Elsevier in MATERIALS & DESIGN on 27 april 2018, available online:www.elsevier.com/locate/matdes https://doi.org/10.1016/j.matdes.2018.04.063."

Facile design of "sticky" near superamphiphobic surfaces on highly porous substrate

Yijian Cao[a,b]; Antonella Salvini[b]; Mara Camaiti[a*]

[a] CNR-Institute of Geosciences and Earth Resources, Via Giorgio La Pira 4 - 50121, Florence, Italy, e-mail: yijian.cao@unifi.it;
[b] Department of Chemistry, University of Florence, Via della Lastruccia 3-13, 50019, Sesto Fiorentino (FI), Italy, e-mail: antonella.salvini@unifi.it.
* Corresponding author: mara.camaiti@igg.cnr.it; Via Giorgio La Pira, 4 - 50121 Florence (Italy); phone: +39-055-2757558.

Abstract

Several “sticky” near superamphiphobic surfaces were fabricated on naturally porous and rough substrate by simply deposing oligoamides solutions, needless of surface modification or integrating nano-materials. These surfaces exhibit very high water and oil contact angles (water contact angle>150°, oil CA>140°) together with high sliding angles (>90°). The nanomaterial-free coating compounds are well-defined, homologous partially fluorinated oligoamides (synthesized via condensation reactions) which have consistent but slightly varied properties, in terms of contact angle and contact angle hysteresis. These surfaces show very high adhesion force to water droplets; in essence, the strong adhesion force is owing to the combination of capillary force derived from newly generated micro-porosity of substrate and the interaction between amidic groups of coating and water molecules. Besides, they exbihit high stability and durability after short and long time water immersion test. This approach may provoke new ideas for creating superamphiphobic surfaces with special adhesion properties on porous substrates. Moreover, these materials could also be potentially employed as water repellents for porous building materials, since they are easy to handle and soluble in environmentally benign solvents. In addition to very high water inhibition efficiency, they manifest high residual vapor permeability and preserve the physical characteristics, i.e. vapor diffusivity and chromatic features, of substrate.

Keywords: Superhydrophobic effect, near superoleophobic effect, high water adhesive force, surface treatment, oligo(ethylenesuberamide); perfluoropolyethers.

1. Introduction

Over the last two decades, bioinspired ultra water repellent surfaces, namely “lotus effect” and “rose petal effect” surfaces have attracted great interest, and extensively successful biomimic surfaces have been developed and studied [1-6]. With static water contact angle (CA) higher than 150° and low contact angle hysteresis (CAH, < 10°), water droplets on lotus leaf could easily roll off (“self-cleaning” effect). Droplets in “lotus effect” are in the Cassie-Baxter state as they suspend on the air-pockets trapped by the microstructure [7-9]. While on rose petals, where droplets are in the Cassie impregnating wetting state, water droplets are tightly pinned at the interface due to the strong adhesive force [10-15].

Owing to the great potential in both fundamental research and functional application, e.g., liquid transport without loss or contamination in microsample analysis [16], dew collection [17] etc., recently, much effort have been devoted to designing “sticky” superhydrophobic surfaces. In order to tune the adhesion forces (AFs) on superhydrophobic surfaces, a series of fabricating methods, such as hydrothermal preparation [18], electro spinning [19], lithography [20], electrochemical deposition [21], solution immersion [22, 23], and so on [24-26], are usually

employed. However, certain limitations e.g., expensive equipment and materials, severe conditions and/or tedious procedures shall be well addressed prior to large scale practical application. It worth noting, besides, these modified surfaces generally originate from flat, smooth substrates (e.g., glass, silicon wafer, metal/alloy foil etc.), yet there is few report describing highly sticky superhydrophobic surfaces generated on naturally porous and rough substrates.

Perfluoropolyethers (PFPEs), a special class of fluoropolymers, with their unique physicochemical properties e.g. low surface energy, high chemical and thermal stability, high gas permeability and low toxicity, have been developed and used as lubricant oils in harsh environment as early as 1960s [27, 28]. Acting as low surface tension (γ ~16-21 mN/m) coating materials, PFPEs and their derivatives are also used in achieving "lotus-effect" and/or oleophobicity [29-33]. It is in common that nanoparticles were employed in theses fabrications to create a dual-hierarchical roughness which is one of the two primary requirements for constructing artificial ultra-repellent surfaces. Nanoparticles do play an indispensable role in these syntheses; however, their fate, stability and toxicity towards human beings and environment are under debate [34, 35].

In previous studies, a series of functionalized PFPEs were used in designing effective water repellents for various building substrates since 1980s [36-39]. In our recent papers [40, 41], two different oligoamides with pendant mono-carboxylic functionalized PFPE blocks demonstrated high water repellency on building stones. In the present paper, herein we report the facile fabrication of "petal effect" near superamphiphobic surfaces on a highly porous, rough substrate (a natural bio-calcarenite) through a simply deposition of a homologous series of partially fluorinated oligoamides. In specific, the PFPE segments-containing oligoethylenesuccinamide (FSC) and -adipamide (FAD), already known as water-repellent for stone substrates [40, 41], and a new oligoethylenesuberamide (FSB) were used as coating materials, and their chemical-physical properties and performance were compared. As a matter of fact, the as-prepared near superamphiphobic surfaces show strong AF to water droplets at the interface. The distinct properties and performance of each created surfaces, in terms of water/oil CA, CA hysteresis, AFs, as well as CA, CA hysteresis and AF fluctuations as products amount changes, were also investigated and studied. It is worth noticing that the surface roughness and surface free energy are modified simultaneously by this approach without introducing nanoparticles or surface processing. To our best knowledge, this is one of the very few papers describing petal-state superamphiphobic surfaces obtained on a naturally porous and rough substrate, and besides, one of the few papers discussing sticky and amphiphobic surfaces derived from materials that incorporate PFPEs. The stability and performance durability of these super-repellent surfaces were also verified by water immersion test (from 2 hours to 24 hours). To evaluate their performance as coating materials, a series of standard tests and measurements were also carried out. In addition to good water absorption inhibition, the original physical properties of rock i.e., vapor diffusivity and chromatic features, were also well preserved as required in some applications. Results of CA measurement and SEM analysis show that the naturally porous microstructures of stone substrate have been modified by products at nano to micrometer levels, giving rise to a hierarchical structure with multi-level roughness. Moreover, the strong capillary force generated by the micro-pore structure of substrate and the hydrogen bonds between amidic groups and water molecules are the key factors responsible for high AF. With these favorable characteristics, our simple surface treatment approach shines new insight into developing "sticky" superamphiphobic surfaces on porous substrates e.g., natural/artificial stones, ceramics,

wood, fabrics etc. Further, owing to the good solubility in friendly solvents for human and environment, durable high water inhibition efficacy, good maintenance of vapor diffusivity and surface color effects of substrate, these coating materials are also good candidates as hydrophobes for building stones.

2. Experimental

2.1 Materials

Ethylenediamine (>99.5%) was purchased from Fluka. Diethyl succinate (99%), diethyl adipate (99%), suberic acid (98%), Tetrahydrofuran (>99.9%) and 2- Propanol (>99.5%) were purchased from Sigma-Aldrich. Absolute ethanol, acetone and anhydrous diethyl ether are products of J. T. Baker. Galden acid (monocarboxylic PFPE acid with $\overline{M_n}$ ≈880 determined by end group alkali titration) and 1,2,2-trichloro-1,1,2 trifluoroethane (A113) were kindly supplied by Ausimont S.p.A. A113 was distilled before use, while all the other chemicals were used as received without further purification.

Ethyl ester of Galden acid was prepared by esterifying the acid with absolute ethanol according to the method described in the literature [39]. Diethyl suberate was obtained by direct esterification with sulfuric acid as catalyst [42].

2.2 Synthesis of fluorinated oliogoamides

2.2.1 Synthesis of oligosuberamide (SubC2)

The oligosuberamide was prepared by modifying the method previously reported in the literature [40]. In a two-necked 100 ml flask, equipped with a reflux condenser and a dropping funnel, ethylenediamine (1.74 ml, 26.07 mmol) was introduced in nitrogen atmosphere and room temperature. Under vigorous magnetic stirring, diethyl suberate (2.000 g, 2.04 ml, 8.68 mmol) and then 2-propanol (2.00 ml) were added dropwise through the dropping funnel. The temperature was raised up to 80-85 °C and kept at this temperature for 12 h. After evaporation of solvent, the solid obtained was washed with 10 ml of diethyl ether for 4 times and then dried under vacuum. The white solid (1.850 g, yield 72%) was characterized by FT-IR ^{1}H- and ^{13}C-NMR spectroscopy. The number-average molecular weight, estimated by ^{1}H-NMR spectroscopy, was 296 g/mol. The detailed characterization of SubC2 is reported in Supplementary Material (SM): “Materials Characterization”.

2.2.2 Synthesis of partially fluorinated oligosuberamide (FSB)

The fluorinated oligosuberamide was prepared by modifying the method previously reported in the literature [40]. In a two-necked 100 ml flask, 2-propanol (15 ml) was added to SubC2 (0.167g, 0.56 mmol) under nitrogen atmosphere and vigorous magnetic stirring. When SubC2 was almost completely dissolved, ethyl ester of Galden acid (1.027 g, 1.13 mmol) was introduced dropwise. The mixture was stirred for 20 h at room temperature before heating up to 65-70 °C for 40 hours. The slightly yellowish waxy product (0.890 g, yield 77%) was recovered

after solvent evaporation under reduced pressure and purification with A113 for 3 times. The product was characterized by FT-IR, ^{1}H- and ^{19}F-NMR spectroscopy. The detailed characterization of FSB is reported in SM: "Materials Characterization".

The syntheses of partially fluorinated oligoadipamide (FAD) and oligosuccinamide (FSC) were performed according to the reported methods [40, 41]. FAD and FSC were also characterized by FT-IR and NMR (^{1}H, ^{13}C, ^{19}F) spectroscopy (in SM: "Materials Characterization").

2.3 Instruments for fluorinated oligoamides characterization

A Perkin Elmer (Spectrum 1000) spectrometer was used to record the FT-IR spectra in the mid-IR range (4000 cm^{-1} to 400 cm^{-1}) in transmission mode with 16 scans and 2 cm^{-1} spectral resolution. KBr windows were used as sample holder. ^{1}H- and ^{13}C-NMR spectra were obtained with a Varian Mercury VXR400 operated at 399.921 MHz and 100.571 MHz respectively, while ^{19}F-NMR spectrum was obtained with a Bruker Avance III 40 operated at 376.5 MHz. ^{1}H-NMR and ^{13}C-NMR shifts are reported in ppm relative to tetramethylsilane (TMS) at 0 ppm, and ^{19}F-NMR shifts are reported in ppm in respect to $CFCl_3$ at 0 ppm.

2.4 Stone materials and products application

Lecce stone, a fine bio-calcarenite, is widely used in southern Italy as constituent material of large-scale architecture since ancient times. It has a rough, beige surface, characterized by homogeneous and fine grains (grain size distribution between 100 and 200 μm) between which microfossils are commonly seen. The water porosity is around 35-47%, with pore size ranging from 0.01 to 2 μm [43-45]. Lecce stone samples were selected and tested based on three sequences of water absorption tests conducted under the guidance of standard method [46]. Specimens that demonstrated constant water absorptivity were chosen. Samples were previously cut into 3·2·0.2 cm^3 slices and 5·5·2 cm^3 slabs.

Aiming at investigating the relationship between product amounts and hydrophobicity, various quantities (i.e., 5.8 g/m^2, 11.1 g/m^2, 18.3 g/m^2 and 22.9 g/m^2) of FSC, FSB and FAD (0.5% w/w 2-propanol solutions) were applied on one larger face of the slices by using a pipette with the method "wet on wet". A pipette is used when small areas must be coated with well defined amount of product. The treatment can be equated to a brush coating. "Wet on wet" is a technique mostly used in stone consolidation, in which additional treatment was applied to previously executed wet surface.

To test their performance as hydrophobic coating, the products were also applied on slabs. 1% (w/w) 2-propanol mixtures of FSC, FSB and FAD were prepared. A graduated pipette (0.5 ml) was used for deposing solutions on one larger face of the rocks with the same method "wet on wet". Treatment was stopped before saturation (about 15 g/m^2), considering the best CA results observed on slices. The exact amount applied was calculated as the weight difference between dry weight before treatment and after treatment. After treatment and before subsequent tests, all treated samples (three slabs and one slice per product), together with the references, were left under laboratory conditions for solvent evaporation (typically one week) and then put in desiccator until a constant weight was reached.

2.5 Coating characterization and measurements

CA of neat and FSC, FSB and FAD coated Lecce stone slices were measured using a Ramè-Hart Model 190 CA Goniometer. Static CA of 5 µl sessile droplets of liquid on stone surfaces was measured. Deionized water and extra virgin olive oil were employed as liquids for CA measurements. The contact angle reported is the average of five discrete drops per sample at different locations. For CA hysteresis measurement, a KRÜSS DSA 30 CA system was employed. Advancing or receding CA was measured by increasing or decreasing the volume of the water droplet deposited on the surface with a small syringe and was recorded when the contact line began to advance or retract. Droplets of 6 µl with an increase of 2 µl for the advancing CA measurements were used. The CA hysteresis was defined as the difference between advancing and receding CA. The AF of superhydrophobic surfaces was estimated by simple calculation based on the maximum volume of water droplet (released from a micro syringe) that can pin at interface. AF was calculated as AF(N) = mass • g, where mass is the weight of water droplet, g = 9.8 m/s^2 is the standard acceleration in free fall.

The surface morphology and elemental mapping analysis of virgin and coated slices were analyzed at Ce.M.E - ICCOM (Florence) by employing an environment scanning electron microscopy (ESEM Quanta – 200 FEI) equipped with an energy - dispersive x-ray spectrometer (X-EDS). Images in secondary (LFD) and backscattered electrons (BSE) were acquired, and elemental composition was obtained working at pressure of 1.00 and 0.50 Torr with a voltage of 25 KeV. Elemental mapping, both on surface and in depth (stratigraphy), was also done at 25 KeV with an amplification time of 10 µs. 11 frames of scan were performed. Mapping on slice treated with 18.3 g/m^2 of FSB was done at MEMA (University of Florence) using a Zeiss EVO MA 15 SEM equipped with an RSD detector and Oxford INCA 250 X-EDS operated at 20 KeV, pressure of 1 Torr and current of 2.4 µA. The stratigraphic elemental mapping analysis was conducted on the internal cross section surface of slices obtained by breaking the slice gently by hand.

The water evaporation process on coated surfaces was evaluated by taking micrographs during evaporation of a 1 µl droplet over time. Photos were taken at different intervals until complete evaporation. The CA, contact diameter was recorded. The stability and durability of several superhydrophobic surfaces with high AF were evaluated by immersing them thoroughly in deionized water for 2, 8 and 24 hours. The CA and AF were measured after each test, after drying the samples.

The water absorption by capillarity, before and after samples treatment, was evaluated according to standard method [46], and the results was processed and reported as water absorption inhibition efficiency (WIE) as described before [41]. The chromatic changes induced by coating were examined by colorimetric analysis [47]. A portable X-Rite SP60 spectrophotometer in specular component excluded mode was employed. For each sample, three measurements were done on a specific spot previously located by using a mask. Results were elaborated and reported in CIE-L*a*b* standard color system, and the color alteration (ΔE*) was calculated [40]. To determine the vapor flow (vapor diffusivity) through the coated stone, the standard "Cup" method was followed [48]. The percentage residual diffusivity, RD (%), through the coated and uncoated rocks was calculated accordingly [41]. Moreover, the effective diffusion coefficient (D_{eff}) of coated stone samples was assessed, by plotting the weight of "Cup" versus time and exploiting Fick's law of diffusion. On the basis of Fick's Law, the molar flux of gas J (moles/area/time), in the steady-state diffusion through a polymeric film is defined as:

$$J = D\frac{(c_1 - c_0)}{L} \quad (1)$$

where D is the diffusivity of gas in the polymer, c_1 and c_o ($c_1 > c_o$) are the concentration of gas at the two ends of the polymeric film with a thickness of L. In the system of "Cup", where normal pressure and temperature are used, a similar situation is observed: the gas is represented by vapor, c_1 and c_o are the concentration (or partial pressure) of vapor (calculated at 30°C) inside and outside the cup, respectively. L is the thickness of the rock slab [49]. In these conditions, the gas diffusion is controlled by molecular diffusion within the gas-filled pores rather than by collisions with pores, and the diffusive flux of vapor through the porous medium was expressed as:

$$J = D_{eff}\frac{(c_1 - c_0)}{L} \quad (2)$$

where D_{eff} is the effective diffusion coefficient, and it was related to the molecular diffusion coefficient of vapor D, the porosity ε and tortuosity τ of the porous material,

$$D_{eff} = \frac{\varepsilon}{\tau}D \ (\tau > 1) \quad (3)$$

3. Results and discussion

3.1 Synthesis and characterization of fluorinated oligoamides

The synthesis of the new fluorinated oligosuberamide was realized via two-step poly-condensation reactions, according to the method previously described [40, 41]. Different reaction conditions were adopted depending on the dicarboxylic acid used (Table S1). The chemical structures of coating materials are shown in Scheme 1. The specific characteristics of the different products are compared and discussed on the basis of the dicarboxylic acid present in the structure. In all the syntheses, an excess of ethylenediamine was used to obtain oligomers with terminal amine groups [40]. However, the molar ratio between esters and ethylenediamine were different, being 1:3, 1:2 and 1:5 for oligosuberamide (SubC2), oligosuccinamide (SucC2), oligoadipamide (ADC2) and, respectively. Reaction time also differed. In fact, SucC2 was obtained within the shortest time (7 h) whereas 22 h were used for synthesizing ADC2. With the shortest reaction time, SucC2 also had the highest yield among all. This is probably due to the varied solubility of oligoamides in the solvent used in the synthesis, and to the possibility to form intra/inter-molecular hydrogen bonding between NH of amidic groups and C=O of carbonyl or of not reacted carboxylic groups. Constituted of four carbon atoms, which is the shortest chain among these three esters, diethyl succinate is less flexible than adipate and suberate, and more likely to form intra-molecular hydrogen bonding, giving rise to a high yield within short time. The reaction was monitored by FT-IR spectroscopy periodically, and special attention was paid on the characteristic absorption bands, e.g., carbonyl groups of ester and amide. These oligoamides are homologous, with slightly differed band positions of functional groups (Table 1). The peak position of amide I (C=O stretching) varied for about 4-5 cm^{-1} from one to another. Specifically, amide I had its absorption band at the highest wavenumber in ADC2 (1637 cm^{-1}) and the lowest wavenumber in SucC2 (1631 cm^{-1}). Additionally, the peak of amide II (C-N

stretching) in ADC2 (1441 cm^{-1}) was at a lower wavenumber than it is in SucC2 and/or SubC2 (1448 cm^{-1}).

The number-average molecular weight ($\overline{M_n}$) of oligoamides was estimated (Table 2), exploiting the method previously reported [40]. All the oligoamides had low molecular weight (~ 300 g/mol), providing sufficient solubility for subsequent reactions. In specific, among all products with similar average molecular weight, the newly synthesized SubC2, showed the highest solubility percentage for a concentration of 1% (w/w) solute/solvent in all tested solvents (Table 2). Whereas, SucC2 is the least soluble one and ADC2 is intermediate.

Table 1 Assignments of the main FT-IR absorption peaks of oligoamides.

Product	Absorption (cm^{-1})					
	ν_{N-H}	ν_{C-H}	$\nu_{C=O}$	δ_{N-H}	ν_{C-N}	ν_{C-F}
SubC2	3300(s)	2935(s)	1634(s)	1550(s)	1448(s)	/
	3076(m)	2861(m)				
FSB	3300(s)	2937(s)	1706(s)	1559(s)	1450(s)	1400-900(s)
	3085(m)	2858(m)	1642(s)			
ADC2	3295(s)	2938(s)	1637(s)	1554(s)	1441(s)	/
	3082(m)	2857(m)				
FAD	3296(s)	2949(s)	1705(s)	1559(s)	1440(s)	1400-900(s)
	3089(m)		1641(s)			
SucC2	3295(s)	2940(s)	1631(s)	1561(s)	1448 (s)	/
	3084(m)	2938(m)				
FSC	3295(s)	2936(s)	1703(s)	1556 (s)	1448 (s)	1400-900(s)
	3084(m)	2890(m)	1636(s)			

s=strong; m= medium

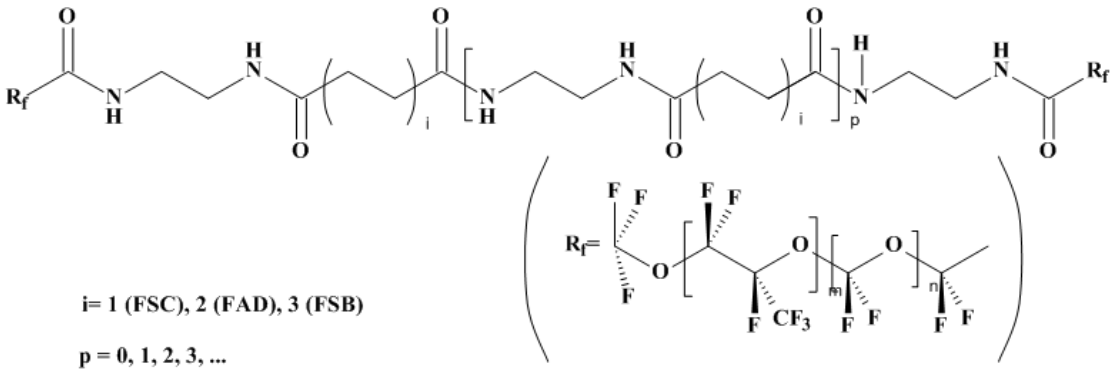

Scheme 1 Chemical structures of FSC, FAD and FSB fluorinated coating materials

Table 2 Percentage of oligoamide dissolved for a specific concentration (1% w/w solute/solvent).

	SubC2		ADC2		SucC2	
$\overline{M_n}$ (g/mol)	296		296		330	
Solvent	Cold	Hot	Cold	Hot	Cold	Hot
H_2O	100 ±3	100 ±0	100 ±4	100 ±0	100 ±5	nd
Ether	0 ±0	nd	0 ±0	nd	0 ±0	nd
THF	20 ±5	60 ±5	0 ±0	nd	0 ±0	15 ±5
Ethanol	80 ±3	nd	20 ±4	nd	0 ±0	nd
2-propanol	80 ±2	100 ±0	15 ±5	80 ±3	0 ±0	20 ±5
2-propanol/ H_2O (70:30)	100 ±0	nd	50 ±5	nd	0 ±0	70 ±4
2-propanol/ H_2O	90 ±3	nd	20 ±5	nd	0 ±0	40 ±5

(90:10)

nd = not determined.

In the second step, reaction conditions were similar for all syntheses, and the molar ratio between oligoamides and ester of PFPE was the same i.e., 1:2 (Table S2). A higher yield (90%) was achieved in synthesizing FAD. During the reaction, attention was drawn on the peak features of amide I in FT-IR spectra, as a strong peak attributing to the amidic groups connected with PFPE segments appeared. Besides, the disappearance of C=O stretching of PFPE ester (1792 cm^{-1}) was also monitored. For all products, the absorption band positions of amide I of the amidic group that connects PFPE chains are very similar, being around 1705 cm^{-1} (Table 1). The peak positions of amide II are relatively constant. Yet, the absorption band position of amide I of the amidic group of internal oligoamide backbones has changed. In specific, all the peak positions of amide I have shifted towards higher wavenumbers, i.e., shifted from 1634 to 1642 cm^{-1}, from 1631 to 1636 cm^{-1} and from 1637 to 1641 cm^{-1} for amide I in FSB, FSC and FAD, respectively. These results indicate the chemical properties of oligoamide backbones have been modified, due to the presence of PFPE segments, resulting in bond energy enhancing of amidic groups.

Although FSB, FAD and FSC are homologous compounds with similar molecular weight (~2000 g/mol), they show distinct solubility behaviors (Table 3) in some organic solvents. The new product FSB has very good solubility in alcoholic and hydro-alcoholic solvents at room temperature, while FSC is soluble only at hot condition and remains partially soluble when the solution was cooled down to room temperature [41]. FAD has intermediate solubility. The solubility variations, which may induce different properties or performance in surface treatment, are closely related to the length of alkyl chains derived from dicarboxylic acids.

Table 3 Average molecular weight ($\overline{M_n}$) and solubility of FSC, FSB and FAD on several solvents. The solubility was determined as percentage of oligoamide dissolved for a specific concentration (1% w/w solute/solvent).[AS1]

	FSB		FAD		FSC	
$\overline{M_n}$ (g/mol) (by ^{1}H-NMR)	2056		2096		2090	
Solvent	Cold	Hot	Cold	Hot	Cold	Hot
Ether	0 ±0	nd	0 ±0	nd	0 ±0	0 ±0
THF	30 ±5	60 ±4	nd	nd	0 ±0	60 ±4
Ethanol	100 ±0	nd	90 ±3	100 ±0	30 ±5	100 ±2

2-propanol	100 ±0	100 ±0	80 ±3	100 ±0	50 ±4	100 ±2
2-propanol/ H_2O (70:30)	70 ±4	100 ±0	50 ±4	90 ±2	50 ±4	100 ±3
2-propanol/ H_2O (90:10)	90 ±3	nd	nd	nd	50 ±4	nd
A113	80 ±3	nd	0 ±0	nd	0 ±0	nd
A113/ 2-propanol (90/10)	90 ±2	nd	nd	nd	0 ±0	nd
A113/ 2-propanol (10/90)	100 ±2	nd	nd	nd	0 ±0	nd

Cold = 20-25°C; Hot = 60-65°C; nd = not determined.

3.2 Wetting property and morphology

Although the surface tension of the oligoamides bearing short PFPE pendant groups (FSC, FAD and FSB) is not known, this is not expected to be very different from that of PFPEs with branched structure (16-18 mN/m) [50]. Considering that the surface tension of water (73 mN/m [51]) and olive oil (32 mN/m [52]) is much higher than that of PFPEs, and the surface has a natural roughness, necessary condition to make super oil/water repellent surfaces [53-55], the wetting properties of the coated stone substrate are assumed to be strongly modified. Moreover, as the amount of fluorinated oligoamides applied on the stone reflects the degree of coverage of the stone surface, a decreasing of the actual surface tension of the coated rock and an increase in water and oil CAs with an increase of product applied are expected [56].

Plots of water and oil CAs versus product amounts are shown in Figure 1. In general, peak values exist for all coatings, before reaching the apexes both water and oil CAs increase as the increasing of product quantity applied. Yet, once the peak value is reached, CA tends to stabilize. The static oil and water CA on neat substrate is 0° and 35°, respectively. When 11.1 g/m^2 of FSC was applied (coating "FSC-11"), a near superamphiphobic surface was generated, on which the static water and oil CA is 154.1±2.4° and 142.1±1.7°, respectively. By quadrupling the original water CA, FSC-11 has modified the wetting property of the neat substrate dramatically. On the surface treated with the same amount of FSB (coating "FSB-11") and FAD (coating "FAD-11"),

though the same rising of water and oil CA is observed, superhydrophobic surfaces were not created. Another near superamphiphobic surface was realized by applying 18.3 g/m^2 of FSB (coating "FSB-18"), with the water and oil CA of 153.2±2.9° and 140.1±2.1°, respectively. However, when the amount of product applied was further increased, higher water and oil CAs were not observed for all coating materials. For FSC and FSB coatings made by 22.9 g/m^2 of product (coating "FSC-22" and "FSB-22"), both their water and oil CAs reduced slightly, being 152.6°, 136.5° for FSC-22 and 152.2°, 132.3° for FSB-22, respectively. Contrarily, the water and oil CAs on surface coated with 22.9 g/m^2 of FAD (coating "FAD-22") were enhanced to around 130°. The varied hydrophobic effects observed on the same substrate coated with the same amount of homologous partially fluorinated oligomers may be explained by the different distribution of coating materials on porous surface and partial coverage of the stone surface, which could create micro differences on surface morphology (formation or not of additional roughness). Besides, when high amounts of product are applied, an accumulation of coating on surface and near the pore throats can induce a hierarchical structure, and the segregated hydrophobic perfluorinated chains may be superimposed by oligoamides molecules bearing extended polar chains (Fig. 2). This disorganized conformation may justify the reducing of water and oil CAs.

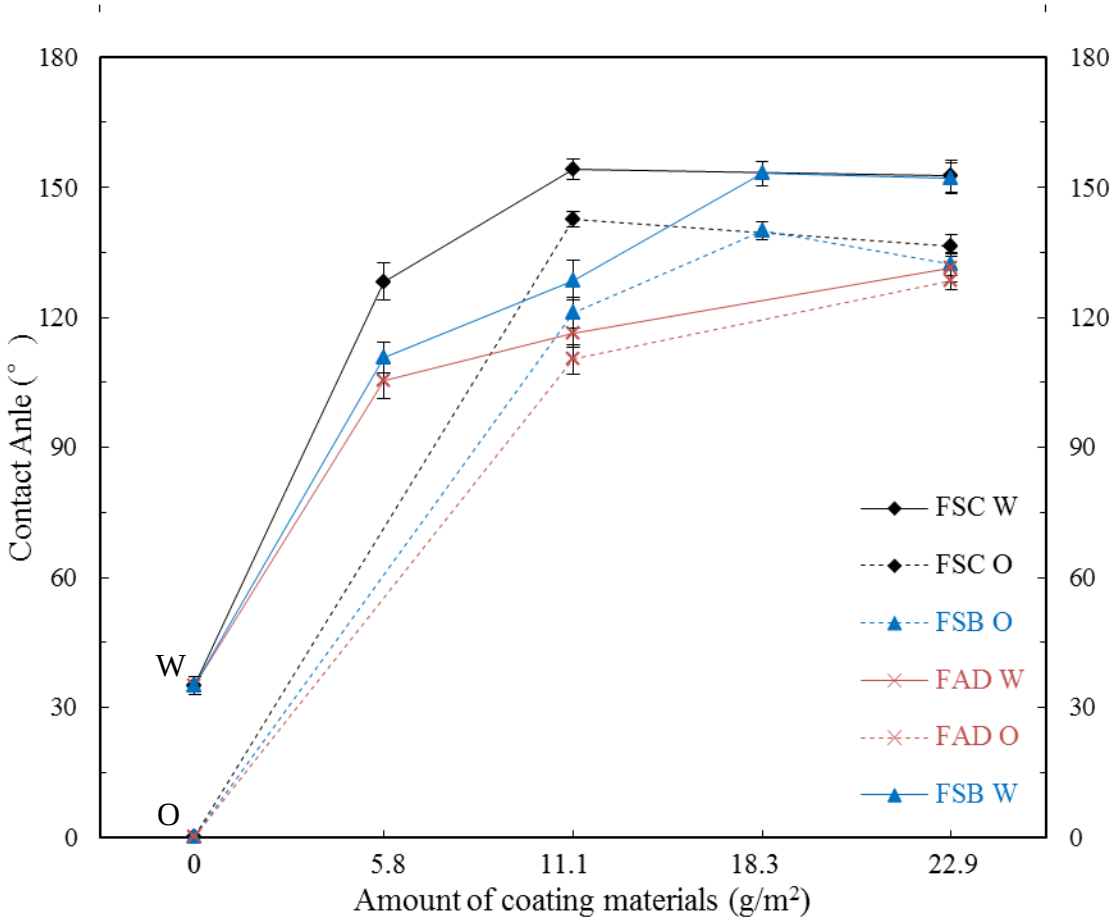

Figure 1 Water (W) and oil (O) Contact angles (CAs) of various coatings.

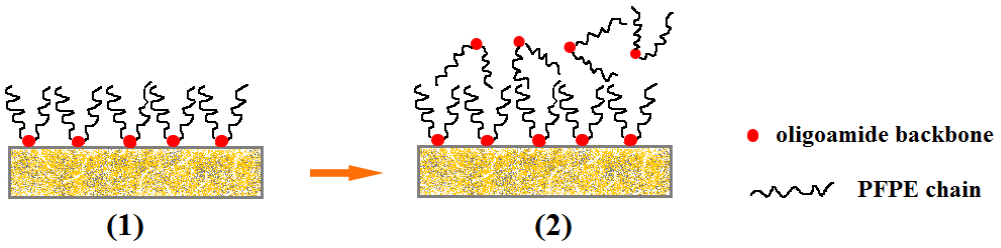

Figure 2 Schematic descriptions of surface orientation of coating materials on porous substrate when the product amount is ideal (1) and oversaturated (2).

In order to verify these assumptions, SEM micrographs of neat and coated stone slices were taken and elemental mapping analysis on both treated and stratigraphic surfaces was also conducted. As shown in Figure 3a, the virgin rock (LS-NT) is very rough and porous. EDS analysis of the surface (rectangular area in Fig. 3a) and fluorine element mapping confirmed that no fluorine is present (Fig. S2). Once 11.1 g/m^2 of FSC were applied, substrate with different surface morphology was observed (Fig. 3b-1 and Fig. 3b-2). Some amorphous, wrenched lamellar-like materials, which partially cover surface and fill in pores are clearly seen on coating FSC-11 (Fig. 3b). The presence of FSC was proved by EDS analysis (Fig. S2). Previous studies have demonstrated that properly controlled surface chemistry and surface microstructure are two indispensable factors for creating ultra-repellent surfaces [54, 55]. In our case, the originally porous surface has been covered by very thin (and probably non-continuous) film as well as by agglomerates and clusters of FSC in dimension varying from nanometer to as large as 120 μm (Fig. 3b). The agglomerates and clusters, indeed, create dual or multi-hierarchically rough microstructures. Additionally, when a thin film is present, the original surface tension is drastically reduced by the PFPE segments of FSC exploiting fluorine surface segregation phenomenon [57-59]. Hence, FSC-11 renders Lecce stone nearly superamphiphobic. The distribution behavior of FSC on substrate was examined by fluorine mapping analysis (Fig. 3b). A large amount of fluorine atoms distributes homogeneously on surface, while in depth the fluorine content is much less; fluorine atoms also distribute uniformly and some atoms have arrived to the bottom. Nonetheless, on coatings made with the same amount of FSB and FAD, different morphologies are seen. Unlike on FSC-11, on FSB-11 and FAD-11, though fluorine atoms with low weight percentages were detected (Fig. S2), no evident coating materials are observed at the same magnification (Fig. 3c and Fig. 3d). In these cases, the oligoamides form a very thin film, which is not visible by SEM analysis. The results of fluorine element mapping are in agreement with the morphologies, i.e., less concentrated fluorine atoms are present on the surface of FSB-11 and FAD-11 (Fig. 3c and Fig. 3d). However, it seems more FSB and FAD than FSC reside in depth, since fluorine atoms are more concentrated in stratigraphy (Fig. 3c and Fig. 3d). Specifically, FAD and mainly FSB tend to gather at the right side of image, which is the direction of treatment and gravity. These distribution and penetration variations can be due to their solubility differences (Table 3). In alcoholic solvents the solubility is FSB>FAD>>FSC. Indeed, FSC easily forms suspension during treatment when the concentration becomes slightly higher than 0.5% as a consequence of solvent evaporation. Therefore, once introduced as

solution, FSB and FAD are more likely to penetrate inside substrate rather than remaining on surface. Hydrophobic surfaces are successfully produced, but the water and oil CAs on FSB-11 and FAD-11 are not as high as on FSC-11 because of lower fluorine content on the surface (partial coverage of the stone surface with a non-continuous coating layer). Moreover, since the original surface texture and microstructure of Lecce stone is microscopically intact, FSB-11 and FAD-11 render the rock surface hydrophobic by mainly fluorine segregation phenomenon. When the amount of FSB and FAD are increased, the fluorine content on surface is also enhanced. In the SEM micrograph of coating FSB-18, some clumps of product spread over the surface and also insert into pores and interstice (Fig. 3e), which is similar to FSC-11, and a similar superhydrophobic effect is achieved. In stratigraphy, FSB penetrated thoroughly, and it is more concentrated in the untreated face (right side) (Fig. 3e). Surface morphologies of FSC-11 and FSB-18 well substantiate the widely acknowledged criteria for achieving superhyophobicity. On coated surface with 22.9 g/m^2 (FSC-22 and FSB-22), similar morphologies as FSC-11 (or FSB-18) were observed, but more product deposing on surface was observed (Fig. S2). This morphology justifies a random distribution of hydrophobic and hydrophilic functional groups of oligoamides, like the illustration in Figure 2-(2). With such disorganized surface orientation, higher water and oil CAs are not expected, and accordingly not found.

In addition to near superamphiphocity, these coatings also exhibit very high AF. On coatings FSC-11, FSB-18, FSC-22 and FSB-22, water droplet pins tightly and does not slide down even when the substrate was tilted vertically or turned upside down (Fig. 4). Meanwhile, the high CA hysteresis (>100°) and low receding angles (≤50°) observed also imply surfaces with high stickiness (Fig. 5). Previous researchers have found, on surfaces where high water adhesion is observed, the three phase contact lines at the liquid/solid interface pin steadily on the surfaces [14, 60]. In order to verify this, the dynamic water CA behaviors and the wetting states of droplet on the coatings were investigated by evaporating experiments with a small water droplet. In Fig. 6, the optical micrographs of a droplet on a FSB coated surface (FSB-22) during varied evaporation time are reported as an example. It is evident that CA decreased rapidly from 151° to around 100° after 12 minutes, and then to less than 10° after 18 minutes. Yet, the three phase contact line (or the contact diameter) kept relatively constant, being μm (start of evaporation) and μm until complete evaporation, thus obeying the so-called "Constant Contact Diameter" mode [60]. Contrary to the superhydrophobic self-cleaning surfaces on which the three phase contact lines are easy to change due to low CA hysteresis, the contact lines pin and the contact area does not shrink on surfaces with high water adhesion [14]. Providing the dual-hierarchically rough surface, air pockets trapped inside are impregnable by water, but they prevent the wetting of coating materials and the substrate, displaying the Cassie impregnating wetting state [11, 54] (Fig. 7). For all coatings, the AF increases as the amount of coating material is added. The maximum AF was found for coating FSC-22 and was about 165 μN. This value is higher than the ones reported in recent literature [10, 14]. The different AF are in accordance with their varied CA hysteresis, since FSC-22 and FSB-22 which show higher AF also have much higher CA hysteresis than FSC-11 and FSB-18. Yet, surfaces that exhibit similar AF also have comparable CA hysteresis, e.g., FSC-11 and FSC-18, FSC-22 and FSB-22. To further understand the origin and changes of AF, the physicochemical structure of both coating materials and substrate are ought to be considered. With pore size ranging from 0.01 to 2 μm and water porosity about 40 %, strong capillary force can be generated on Lecce stone surface. Once a relatively high amount of product is introduced, the coatings can not only be distributed in a mono-molecular layer, but also creates an additional microscopic roughness. Coating enters and

covers the pore walls and micro-fissures, which results in partially filling of small pores and in diameter reduction of relatively larger pores. This specific micro-porosity enables strong capillary force as the virgin substrate, which is comparable with the gravity force of water droplets. Similar results have also been found by other researches [61, 62], where the micro-orifices and the wall roughness on surface produces a miniscule capillary force which is sufficient to balance the weight of certain droplets. On the other hand, the fact that the highest AFs were found on coatings FSC-22 and FSB-22, where the CAs were slightly reduced compared with FSC-11 and FSB-18 respectively, shall not be neglected (Fig. 8). An over saturation (i.e., 22.9 g/m^2 of products) of oligoamides actually disrupted the ordered, well segregated hydrophobic PFPE chains which expose outwards at the air-solid interface, thus impairing hydrophobic effect (Fig. 2). Yet, this conformation change enhanced the AF due to the exposure of the polar oligoamides backbones. Each amidic group can form at most four hydrogen bonds with water molecules, among which carbonyl oxygen forms the strongest hydrogen bond with water [63]. Since the superhydrophobic surfaces are in the Cassie impregnating wetting state, water can wet the air pockets trapped inside micro-structures. With an overloading of coating (disorganized structures), the polar amidic groups are more reachable for water molecules, producing stronger hydrogen bonds and facilitating AF. Therefore, the decreasing of CA and the increasing of AF are not contradictory, rather, they are in great harmony. Likewise, the hydrogen bonds formed between hydrophilic nitro groups on the PTES (1*H*,1*H*,2*H*,2*H*-perfluorooctyltriethoxysilane)-NC (nitrocellulose) modified TiO_2 spongelike film and water also provides good adhesion force [64].

In essence, considering the solubility of the fluorinated oligoamides (mainly FSC and FSB), it is possible to tune the near superamphiphobicity by simple deposition of controlled amounts of coating as dilute solution in solvents with a relatively low vapor pressure. Indeed, FSC (the less soluble product) is prone to spread out on the external surface giving superhydrophobicity and near superoleophobicity with small amount of product. On the contrary, FSB (the most soluble product) enters the pores of the rock and forms a dual-hierarchical rough surface with a larger amount of coating than FSC. In case that the AF parameter is more relevant than superamphiphobicity, an oversaturated surface improves its value.

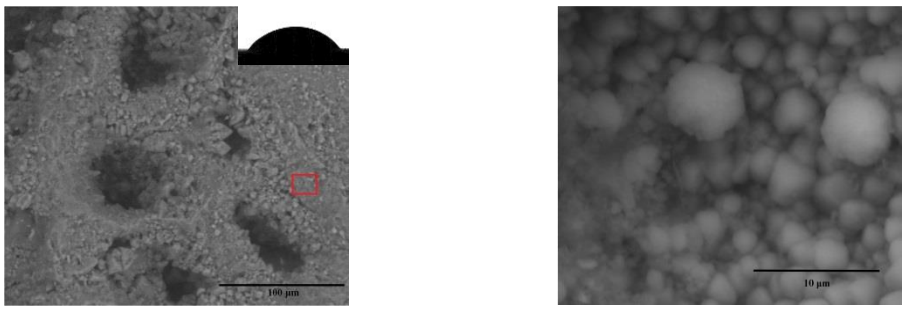

(a) LS-NT

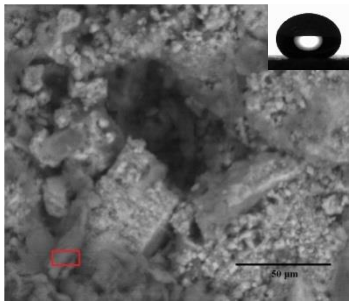

(b-1)

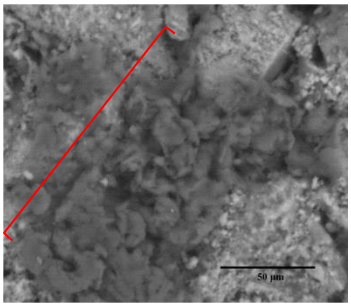

(b-2)

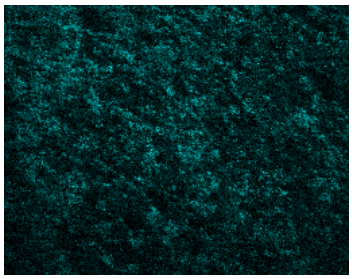

(b-3) Surface F mapping

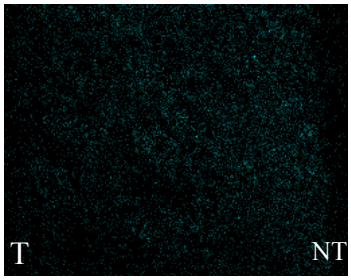

(b-4) Stratigraphic F mapping

(b) FSC-11

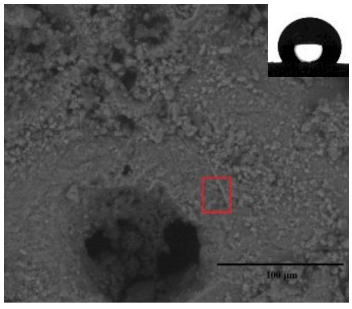

(c-1)

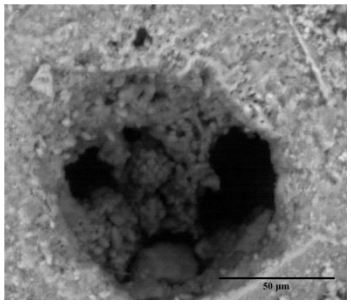

(c-2)

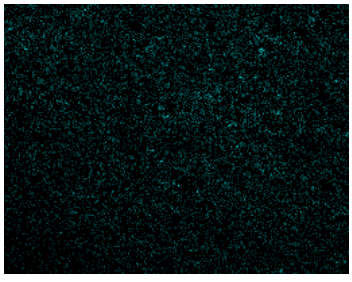

(c-3) Surface F mapping

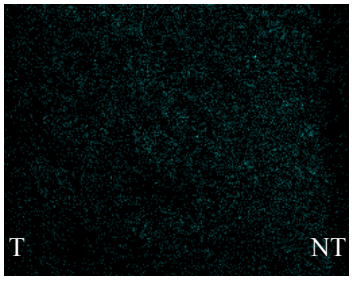

(c-4) Stratigraphic F mapping

(c) FSB-11

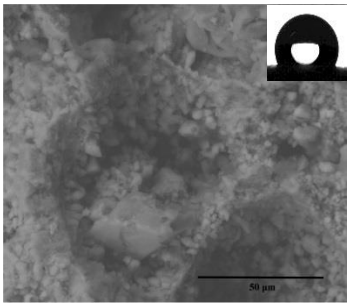

(d-1)

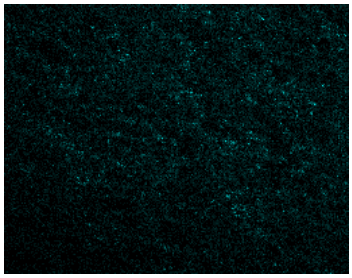

(d-2) Surface F mapping

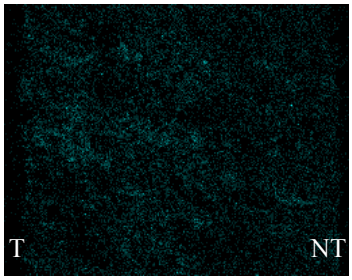

(d-3) Stratigraphic F mapping

(d) FAD-11

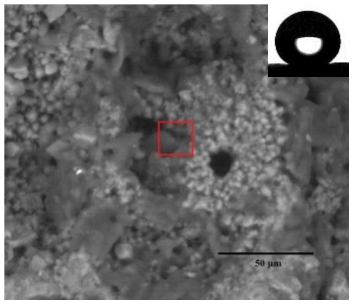

(e-1)

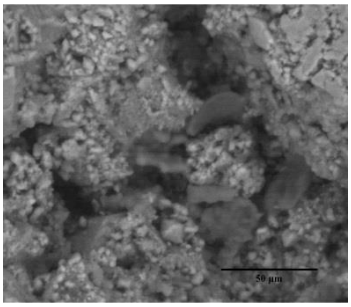

(e-2)

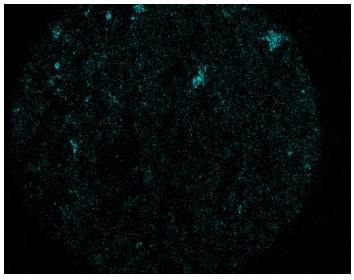

(e-3) Surface F mapping

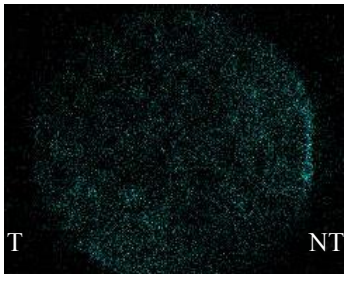

(e-4) Stratigraphic F mapping

(e) FSB-18

Figure 3 SEM micrographs and fluorine maps of not treated (LS-NT) (a), and treated stone substrate with FSC-11 (b), FSB-11 (c), FAD-11 (d) and FSB-18 (e). The insets are images of water CA on corresponding surface. “T”= treated face and “NT” = untreated face.

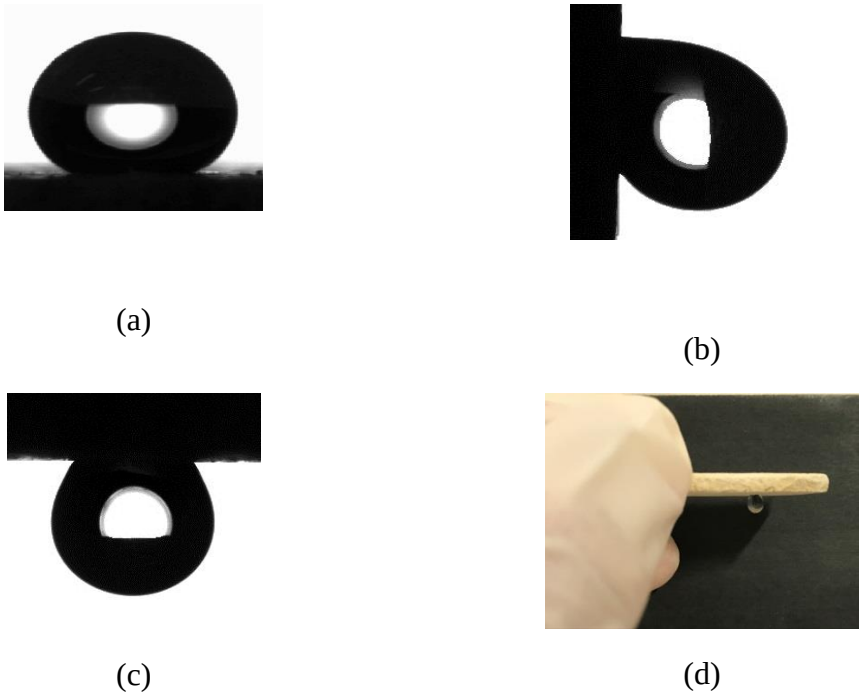

(a) (b)

(c) (d)

Figure 4 Static contact angle of water droplets on FSC-11 with tilt angle of 0° (a), 90° (b) and 180° (c). 17 µl of water droplet pinned on FSC-22 (d).

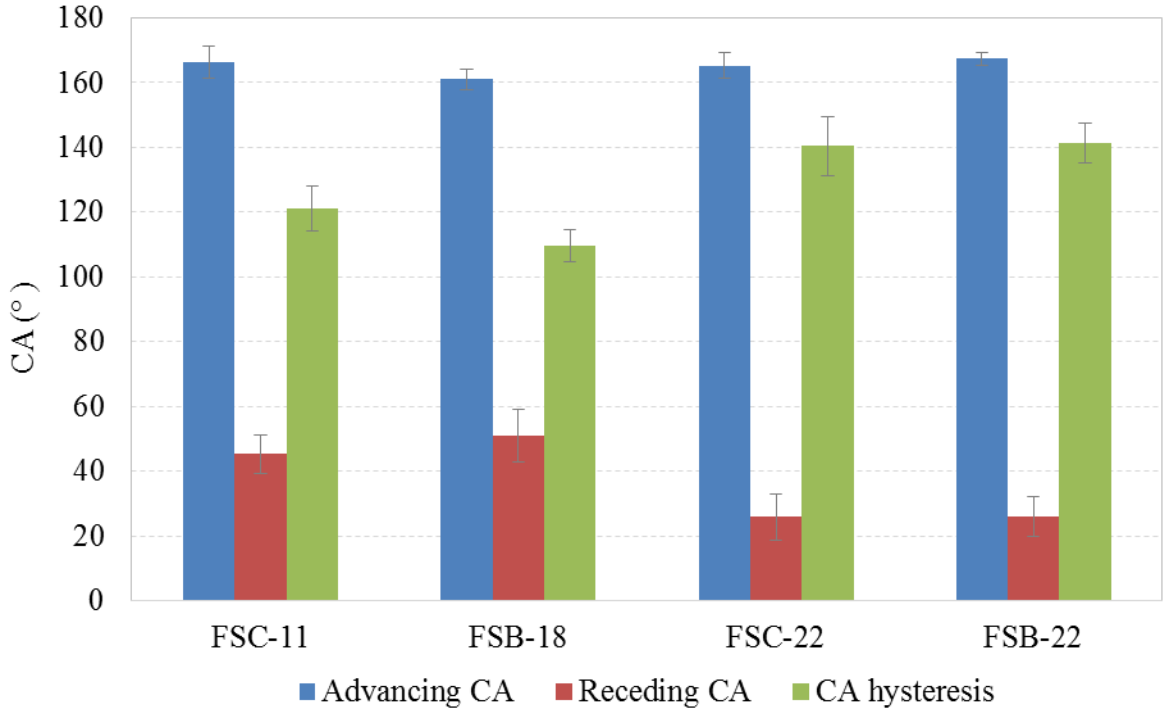

Figure 5 Advancing CA, receding CA and CA hysteresis of FSC and FSB coatings made with different amounts.

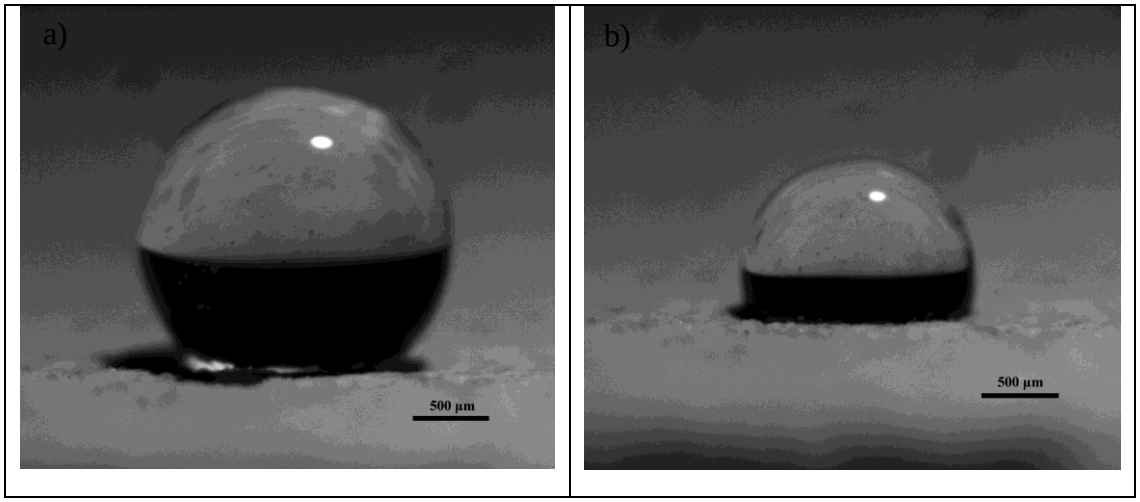

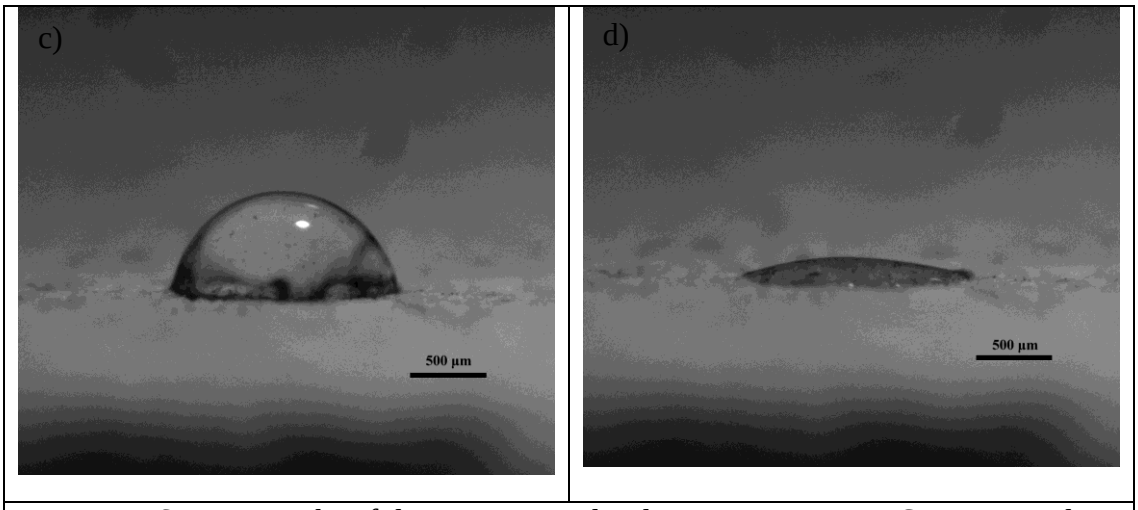

Figure 6 Micrographs of dynamic water droplet evaporation on FSB-22 coated surface after 0 min (a), 12 mins (b), 15 mins (c) and 18 mins (d).

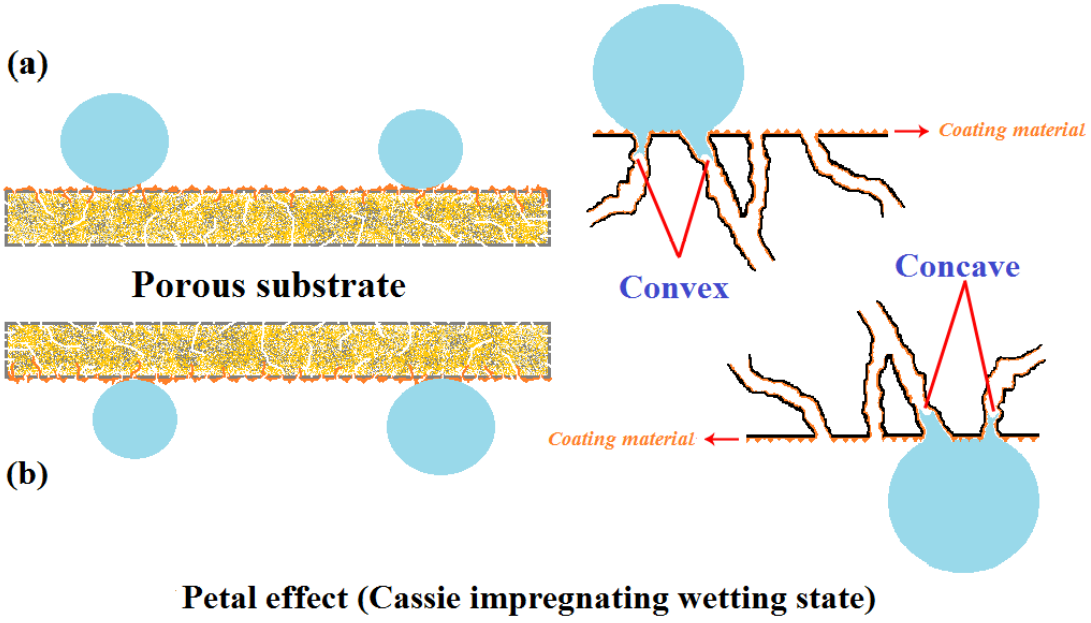

Figure 7 Schematic illustrations of water droplets in contact with the as-prepared adhesive superhydrophobic surfaces at tilting angle of 0° (a) and 180° (b).

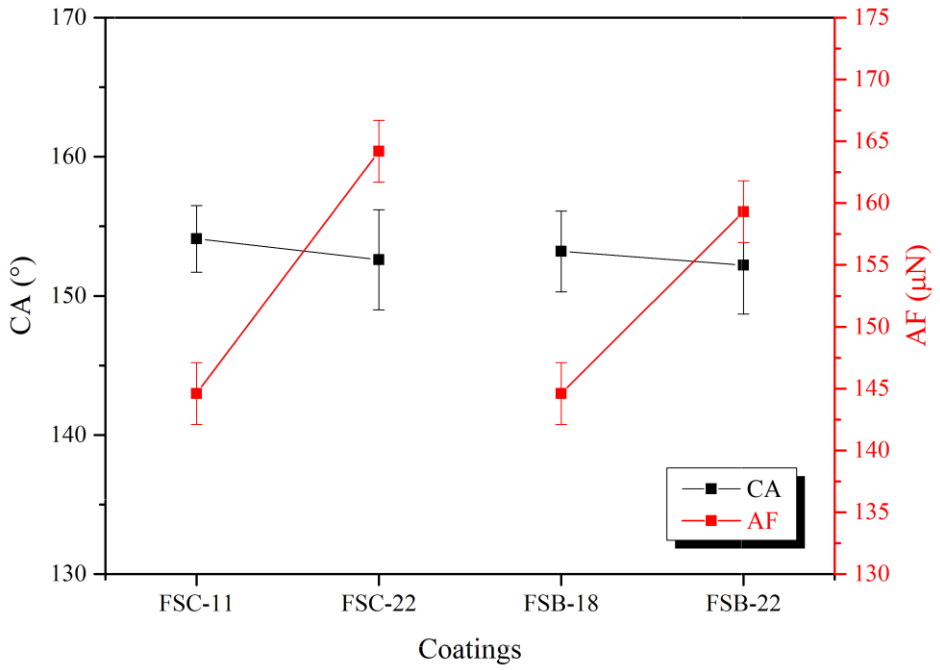

Figure 8 Contact angle (CA) and adhesion force (AF) of FSC and FSB coatings made with different amounts

The stability and durability of these sticky surfaces were also evaluated by means of water immersion test; the CA and AF variations are shown in Figure 9 and Figure S7, respectively. Though the CA of all these four surfaces decreased slightly after immersion, the average CA values are always above 150°, maintaining superhydrophobicity. Further, the AF of all surfaces is relatively durable, and no evident performance decay was seen. Results indicate that the hydrophobic and adhesive properties of these surfaces are stable and durable.

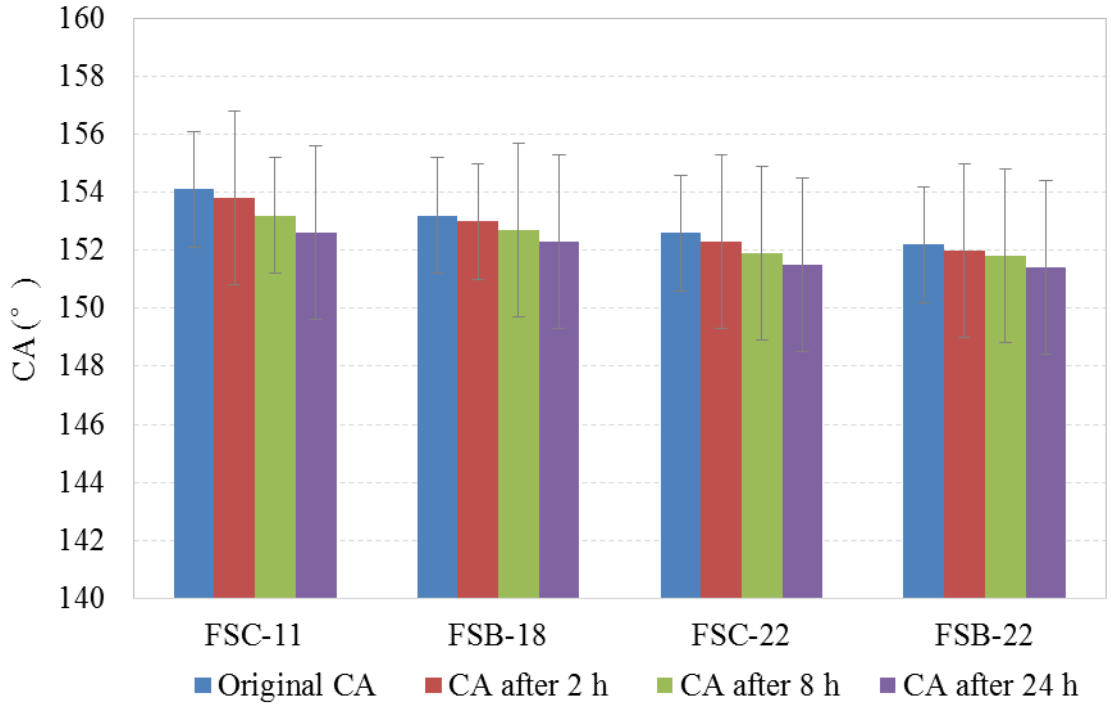

Figure 9 CA variations of sticky ultra-repellent coatings after 2 h, 8 h and 24 h water immersion test.

3.3 Water inhibition efficiency, vapor diffusivity and other performance

To evaluate the physical property changes of substrates after coating by standard tests, products were also applied on slabs. Founded on CA results, the amount of materials was kept to be around 15 g/m^2 to provide the best hydrophobicity. With such quantities applied, FSC and FSB have manifested good hydrophobicity (WIE ≥84%) in two-hour test (Table 4). In particular, FSC has higher WIE values than FSB although its amount applied was slightly lower (13 g/m^2 versus 16 g/m^2). Yet, FAD is not very effective as water repellent for Lecce stone, and its WIE values decreased rapidly to 50% within two hours. These WIE values are in good accordance with the water CA (Fig. 1). As demonstrate by SEM-EDS and fluorine mapping analyses, the best WIE values obtained with FSC coatings owing to its propensity to concentrate at the external surface of slab (i.e., lower penetration depth than FSB and FAD), creating an efficient barrier to liquid water. On the contrary, the better hydrophobic effect of FSB coated surface than the FAD one is not yet well understood, but it might be related to the potential formation of intermolecular hydrogen bonding in the oligoamides solutions with certain length of alkyl chain in the starting dicarboxylic acid; this property can influence the fluorine segregation during the coating process.

Table 4 Water inhibition efficiency (WIE), residual vapor diffusivity (RD) and chromatic changes (ΔE*) of Lecce stone samples coated with fluorinated oligoamides.

	Product quantity		WIE (%) at			RD	ΔE*
	Theoretical g (g/m^2)	Actual g (g/m^2)	30 min	60 min	120 min	(%)	
FSB		0.041±0.003 (16)	92	88	84	96±3.4	3.0
FAD	0.037 (15)	0.037±0.006 (15)	80	69	50	99±2.1	1.5
FSC		0.033±0.005 (13)	95	93	90	97±3.8	2.8

To investigate the vapor diffusivity through neat and coated Lecce stone surface, the standard "Cup" method was exploited. Following this method, the molar flux of water vapor pass through the sample is expressed as the time rate of liquid loss in the system:

$$< J >= D\frac{(c_1 - c_0)}{L} = \frac{moles_{H_2O}}{Area \cdot time} = -\frac{1}{A \cdot M_{H_2O}}\frac{dW_{H_2O}}{dt} \quad (4)$$

where W_{H2O} is the mass of water loss, and M_{H2O} is the molecular weight of water. An example of calculation is given in SM: "Diffusivity computation", along with plots of W_{H2O} versus time for neat and all coated stones (Figs. S3-S6). Using equation (4), the average D_{eff} values found for FSC, FSB and FAD coated Lecce stone are reported in Table 5.

An estimation of D_{eff} can also be computed based on Equation (3), when ε and τ are properly calculated as follows. Since D_{eff} of neat Lecce stone is experimentally known and the diffusion coefficient of vapor in air is also known (D=2.02 *10^{-1} cm^2/sec) from the literature [65], assuming 35% as the average porosity of Lecce stone, the tortuosity of this rock is calculated using Equation (3) (τ= 4.50). The calculated τ is much larger than the value reported in a recent paper (τ=2.32) where relaxation times of NMR were used to calculate the τ providing the time dependence of the self-diffusion coefficient (D) approaches an asymptotic value [66]. There are some reasons accounting for this difference. Based on literature, it is of great difficulty to calculate (or measure) the τ of porous media, whereas the methods to measure D are relatively easier. Tortuosity is usually deduced from the diffusion coefficient [67], but sometimes the tortuosity has been interpreted in conflicting ways [68]. Besides, although the type of our rock is the same as the one used in the explained article [66], the physical properties e.g., porosity and tortuosity of the stone samples quarried from varied quarries can be different.

Table 5 Residual vapor diffusivity (RD), effective diffusivity (D_{eff}) and estimated porosity (ε) reduction of stone samples after coating.

Coating	RD (%)	Experimental D_{eff} @RH%=5% (cm^2/sec)	τ	Estimated ε reduction (%)	Estimated D_{eff}^{*} (cm^2/sec)
Neat	/	$1.57 \cdot 10^{2}$ ±0.05	4.50 (2.32) [66]	/	/
FSB	96	$1.48 \cdot 10^{-2}$ ± 0.06		2.34	$1.47 \cdot 10^{-2}$
FAD	99	$1.54 \cdot 10^{-2}$ ± 0.01		2.11	$1.48 \cdot 10^{-2}$
FSC	97	$1.51 \cdot 10^{-2}$ ± 0.06		1.89	$1.49 \cdot 10^{-2}$

* = D_{eff} was calculated based on porosity reduction; Neat = not treated stone.

Furthermore, the porosity change after coating could be estimated as well. Taking 0.2 cm as the medium penetration depth and 1 g/ml as the lowest density of products, the maximum volume reduction caused by coating materials are 0.033, 0.041 and 0.037 ml for FSC, FSB and FAD, respectively. Presuming 35% as the mean original porosity of substrate, less than 3% of pore space was filled after coating (Table 5). Based on the estimated porosity change and calculated tortuosity, the corresponding estimated D_{eff} is reported in Table 5. Generally, for each coating, the estimated D_{eff} value is slightly reduced, and it is in good agreement with the value measured by the "Cup" method. Among the experimental $D_{eff,}$ a greater tendency to decrease is observed for the FSB treatment; it cannot be explained only with the porosity reduction, since it is the most penetrating product. As presented in a previous paper [41], the vapor diffusion process is compromised by the presence of non-wettable pore walls which restrains the vapor condensation that assists the diffusion process. Therefore, the slightly lower D_{eff} and residual diffusivity are in accordance with the explanation. In any case, however, pore blockage does not occur in all the coating systems.

Last but not least, all the coating materials did not induce any perceivable chromatic changes ($\Delta E \leqq 3$) on surface (Table 4), permitting large area application in practice where color features matter.

The good performance demonstrated by these coatings in terms of efficiency and durability of water inhibition, vapor diffusivity and color features make them eligible products as protective agents for outdoor stone artifacts (e.g. historic buildings, statues). In particular, FSB was proved to be the best coating material because it provides a better hydrophobic effect than FAD, and it has better solubility than FSC. The good solubility in solvents with medium polarity and medium/low vapor pressure, such as alcohols, allows the optimal coating conditions. In fact, a wetting and stable solution favors the homogeneous distribution and penetration of the product inside the pore space, reducing the vapor condensation which is a degradation cause of rocks.

4. Conclusion

Several superhydrophobic surfaces with high adhesion force were prepared, for the first time on naturally rough and porous substrate, by facile solution deposition of oligomers bearing short pendant PFPE chains without any surface treatment process or incorporating nanomaterials. The coatings are also near superoleophobic, and the highest oil CA observed is about 142°. The coating materials, partially fluorinated oligoamides, are homologous compounds with well-defined structures and molecular weight. The sticky ultra-repellent surfaces, with high but varied CAs and AFs, were obtained by applying accurately tunned quantities. The maximum AF assessed, about 165 μN, was found on the stone surface coated with 22.9 g/m^2 of fluorinated oligosuberamide (FSB-22) and oligosuccinamide (FSC-22). Results revealed that the strong AF arises from the combination of capillary force due to the natural and newly created micro-pores and orifices at multiple dimension scales in the substrate, and the hydrogen bonds formed between amidic groups and water molecules. The superhydrophobic and adhesive properties of these surfaces are stable towards short and long time water immersion test. Meanwhile, the original vapour diffusivity of porous substrate (Lecce stone) was well preserved after coating. Indeed, the porosity reduction (< 3%) and vapour diffusivity impairment caused by treatment were merely negligible. In addition, the new products have exhibited good performance as water repellents for highly building materials, since very high hydrophobicity was achieved without inducing sever chromatic change. Complementary to those sticky ultra-repellent surfaces obtained on smooth, flat substrates, our facile methods may shed light on functional applications on porous and rough substrates.

Supplementary data to this article can be found online at http://dx. doi.org…..

Acknowledgement

The authors would like to thank Prof. Rodorico Giorgi and Dr. Emiliano Carretti (Department of Chemistry - University of Florence) and Consorzio per lo Sviluppo dei Sistemi a Grande Interfase (CSGI) for help with the contact angle measurement.

References

[1] X. M. Li, D. Reinhoudt, M. Crego-Calama, What do we need for a superhydrophobic surface? A review on the recent progress in the preparation of superhydrophobic surfaces, Chem. Soc. Rev. 36 (2007) 1350−1368.

[2] X. Zhang, J. Niu, Y. Jiang, Z. Wang, Superhydrophobic Surfaces: From structural control to functional application, J. Mater. Chem. 18 (2008) 621-633.

[3] N. Shirtcliffe, G. McHale, M. Newton, An introduction to superhydrophobicity, Adv. Colloid Interface Sci. 161 (2011) 124-138.

[4] E. Celia, T. Darmanin, E. De Givenchy, S. Amigoni, F. Guittard, Recent Advances in designing superhydrophobic surfaces, J. Colloid Interface Sci. 410 (2013) 1-18.

[5] Z. Chu, S. Seeger, Superamphiphobic surfaces, Chem. Soc. Rev. 43 (2014) 2784-2798.

[6] J. Yong, F. Chen, Q. Yang, J. Huo, X. Hou, Superoleophobic surfaces, Chem. Soc. Rev. 46 (2017) 4168-4217.

[7] W. Barthlott, C. Neinhuis, Purity of the sacred lotus, or escape from contamination in biological surfaces, Planta 202 (1997) 1−8.

[8] X. Wu, Q. Fu, D. Kumar, J. W. C. Ho, P. Kanhere, H. Zhou, Z. Chen, Mechanically robust superhydrophobic and superoleophobic coatings derived by sol‐gel method, Mater. Des. 89 (2006) 1302-1309.

[9] D. Aslanidou, C. Panayiotou, I. Karapanagiotis, Tuning the wetting properties of siloxane-nanoparticle coatings to induce superhydrophobicity and superoleophobicity for stone protection, Mater. Des. 108 (2016) 736-744.

[10] A. Gao, Y. Zhao, Q. Yang, Y. Fu, L. Xue, Facile preparation of patterned petal-like PLA surfaces with tunable water micro-droplet adhesion properties based on stereo-complex co-crystallization from non-solvent induced phase separation processes, J. Mater. Chem. A 4 (2016) 12058-12064.

[11] Y. Lai, X. Gao, H. Zhuang, J. Huang, C. Lin, L. Jiang, Designing superhydrophobic porous nanostructures with tunable water adhesion, Adv. Mater. 21 (2009) 3799−3803.

[12] L. Feng, Y. Zhang, J. Xi, Y. Zhu, N. Wang, F. Xia, L. Jiang, Petal effect: a superhydrophobic state with high adhesive force, Langmuir 24 (2008) 4114−4119.

[13] E. Bormashenko, T. Stein, R. Pogreb, D. Aurbach, "Petal effect" on surfaces based on lycopodium: high-stick surfaces demonstrating high apparent contact angles, J. Phys. Chem. C 113 (2009) 5568−5572.

[14] T. Zhu, C, Cai, J. Guo, R. Wang, N. Zhao, J. Xu, Ultra water repellent polypropylene surfaces with tunable water adhesion, ACS Appl. Mater. Interface 9 (2017) 10224-10232.

[15] M. Chen, W. Hu, X. Liang, C. Zou, F. Li, L. Zhang, F. Chen, H. Yang, A facile all-solution-processed surface with high water contact angle and high water adhesive force, ACS Appl. Mater. Interface 9 (2017) 23246–23254.

[16] X. Hong, X. F. Gao, L. Jiang, Application of superhydrophobic surface with high adhesive force in no lost transport of superparamagnetic microdroplet, J. Am. Chem. Soc. 129 (2007) 1478−1479.

[17] A. R. Parker, C. R. Lawrence, Water capture by a desert beetle, Nature 414 (2001) 33-34.

[18] X. D. Zhao, H. M. Fan, X. Y. Liu, H. Pan, H. Y. Xu, Pattern dependent tunable adhesion of superhydrophobic MnO_2 nanostructured film, Langmuir 27 (2011) 3224−3228.

[19] G. Gong, J. Wu, Y. Zhao, J. Liu, X. Jin, L. Jiang, A Novel fluorinated polyimide surface with

petal effect produced by electrospinning, Soft Mater 10 (2014) 549-552.
[20] X. Huang, D. Kim, M. Im, J. Lee, J. Yoon, Y. Choi, "Lock-and key" geometry effect of patterned surfaces: wettability and switching of adhesive force, Small 5 (2009) 90−94.
[21] Y. Lai, X. Gao, H. Zhuang, J. Huang, C. Lin, L. Jiang, Designing superhydrophobic porous nanostructures with tunable water adhesion, Adv. Mater. 21 (2009) 3799−3803.
[22] S. Wang, L. Feng, L. Jiang, One-step solution-immersion process for the fabrication of stable bionic superhydrophobic surfaces, Adv. Mater. 18 (2006) 767−770.
[23] Z. Cheng, M. Du, H. Lai, N. Zhang, K. Sun, From petal effect to lotus effect: a facile solution immersion process for the fabrication of super-hydrophobic surfaces with controlled adhesion, Nanoscale 5 (2013) 2776−2783.
[24] L. Wang, J. Wei, Z. Su, Fabrication of surfaces with extremely high contact angle hysteresis from polyelectrolyte multilayer, Langmuir 27 (2011) 15299−15304.
[25] J. Li, Z. Guo, J. Liu, X. Huang, Copper nanowires array: controllable construction and tunable wettability, J. Phys. Chem. C 115 (2011) 16934−16940.
[26] D. Ishii, H. Yabu, M. Shimomura, Novel biomimetic surface based on a self-organized metal−polymer hybrid structure, Chem. Mater. 21 (2009) 1799−1801.
[27] W, H. Gumprecht, PR-143—A New Class of High-Temperature Fluids, ASLE Trans 9 (1966) 24-30
[28] L. J. Gschwender, C. E. Jr. Snyder, U.S. Air force perfluoropolyalkylether experiences, STLE Tribology Trans. 52 (2009) 165-170.
[29] L. Zhang, Z. Zhou, B. Cheng, J. M. De Simone, E. T. Samulski, Superhydrophobic behavior of a perfluoropolyether lotus-leaf-like topography, Langmuir 22 (2006) 8576-8580.
[30] Z. Ye, Y. Chen, X. Yang, W. Hu, H. Ye, Development of perfluoropolyether modified raspberry particles with fine hierarchical structure and their application in superhydrophobic surface, Colloids Surf. A Physicochem. Eng. Asp. 514 (2017) 251-259.
[31] Z. Guo, F. Zhou, J. Hao, W. Liu, Effects of system parameters on making aluminum alloy lotus, J. Colloid Interface Sci. 303 (2006) 298-305.
[32] Y. Gao, Y. Huang, S. Feng, G. Gu, F. Qing, Novel superhydrophobic and highly oleophobic PFPE-modified silica nanocomposite, J. Mater. Sci. 45 (2010) 460-466.
[33] E. Sumino, T. Saitoa, T. Noguchib, H. Sawada, Facile creation of superoleophobic and superhydrophilic surface by using perfluoropolyether dicarboxylic acid/silica nanocomposites, Polym. Adv. Technol. 16 (2015) 345-352.
[34] V. K. Sharma, J. Filip, R. Zborilb, R. S. Varma, Natural inorganic nanoparticles – formation, fate, and toxicity in the environment, Chem. Soc. Rev. 44 (2015) 8410-8423.
[35] C. Levard, E. M. Hotze, G. V. Lowry, G. E. Jr. Brown, Environmental transformations of silver nanoparticles: impact on stability and toxicity, Environ. Sci. Technol. 46 (2012) 6900-6914.
[36] F. Piacenti, F. Ciampelli, A. Pasetti, Protecting materials subject to degradation by atmospheric and polluting agents by means of perfluoropolyethers US 4499146 A (1983).
[37] F. Piacenti, A. Pasetti, U. Matteoli, E. Strepparola, Method for protecting stone materials from atmospheric agents by means of perfluoropolyether derivatives US 4745009 A (1986).
[38] U. Matteoli, P. Tiano, A. Scala, M. Camaiti, F. Piacenti, Perfluoropolyethers isobutylamide and isobutylester. Performance in the protection of stones, Proceedings of VIth International Congress on Deterioration and Conservation of Stone, Nicholas Copernicus University-Poland, 1988, 12-14 September, 1988, 509-514.
[39] F. Piacenti, M. Camaiti, Synthesis and characterization of fluorinated polyetheric amides, J.

Fluo. Chem. 68 (1994) 227-235.
[40] Y. Cao, A. Salvini, M. Camaiti, Oligoamide grafted with perfluoropolyether blocks: a potential protective coating for stone materials, Prog. Org. Coat. 111 (2017) 164-174.
[41] M. Camaiti, L. Brizi, V. Bortolotti, A. Papacchini, A. Salvini, P. Fantazzini, An Environmental friendly fluorinated oligoamide for producing nonwetting coatings with high performance on porous surfaces, ACS Appl. Mater. Interface 42 (2017) 37279-37288.
[42] M. A. Ogliaruso, J. F. Wolfe, Synthesis of carboxylic acids, esters and their derivatives, John Wiley & Sons Inc, Chichester-UK, 1991.
[43] S. Bugani, M. Camaiti, L. Morselli, E. V. De Casteele, K. Janssens, Investigation on Porosity changes of Lecce stone due to conservation treatments by means of x-ray nano-and improved micro-computed tomography: preliminary results, X-Ray Spectrom. 36 (2007) 316-320.
[44] S. Bugani, M. Camaiti, L. Morselli, E. V. De Casteele, K. Janssens, Investigating morphological changes in treated vs. untreated stone building materials by x-ray micro-CT. Anal. Bioanal. Chem. 391 (2008) 1343-1350.
[45] M. Gombia, V. Bortolotti, R. J. S. Brown, M. Camaiti, L. Cavallero, P. Fantazzini, Water vapor absorption in porous media polluted by calcium nitrate studied by time domain nuclear magnetic resonance, J. Phy. Chem. B. 113 (2009) 10580-10586.
[46] Norm NUNI-EN 15801-2010, Conservation of Cultural Heritage–Test methods–Determination of water absorption by capillarity, 2010.
[47] Norm UNI-EN 15886-2010, Conservation of Cultural Heritage–Test methods–Measurement of the color of the surface, 2010.
[48] Norm UNI-EN 15803-2010, Conservation of Cultural Heritage–Test methods–Determination of water vapor permeability, 2010.
[49] F. Piacenti, R. G. Carbonell, M. Camaiti, F. E. Henon, E. Luppichini, Protective materials for stone–effects on stone permeability and gas transport, Proceedings of International Colloquium on "Methods of Evaluating Products for the Conservation of Porous Building Materials in Monuments" Roma-Italy, 19-21 June, 1995, 389-402.
[50] T. J. Kałdoński, Ł. Gryglewicz M. Stańczyk, T. Kałdoński, Investigations on lubricity and surface properties of selected perfluoropolyether oils, Journal of KONES Powertrain and Transport 18/1 (2011) 199-212.
[51] N. R. Pallas, Y. Harrison, An Automated Drop Shape Apparatus and the Surface Tension of Pure Water, Colloids Surf. 43 (1990) 169-194
[52] S. N. Sahasrabudhe, V. Rodriguez-Martinez, M. O'Meara, B. E. Farkas, Density, viscosity, and surface tension of five vegetable oils at elevated temperatures: Measurement and modeling, Int. J. Food Prop. 20 (2017) S1965–S1981.
[53] S. Shibuichi, T. Yamamoto, T. Onda, K. Tsujii, Super Water- and Oil-Repellent Surfaces Resulting from Fractal Structure, J. Colloid Interface Sci. 208 (1998) 287-294.
[54] A. Lafuma, D. Quere, Superhydrophobic states, Nat. Mater. 2 (2003) 457−460.
[55] S. Wang, L. Jiang, Definition of superhydrophobic states, Adv. Mater. 19 (2007) 3423-3424.
[56] G.W. Tyndall, P.B. Leezenberg, R.J. Waltman, J. Castenada, Interfacial interactions of perfluoropolyether lubricants with magnetic recording media, Tribol. Lett. 4 (1998) 103-108.
[57] J. Schineider, C. Erdelen, H. Ringsdorf, J. T. Rabolt, Structural studies of polymers with hydrophilic spacer groups. 2. Infrared spectroscopy of Langmuir-Blodgett multilayers of polymers with fluorocarbon side chains at ambient and elevated temperatures, Macromolecules 22 (1989) 3475-3480.

[58] Y. Katano, H. Tomono, T. Nakajima, Surface property of polymer films with fluroalkyl side chains, Macromolecules 27 (1994) 2342-2344.
[59] S. J. Hardman, N. Muhamad-Sarih, H. J. Riggs, R. L. Thompson, J. Rigby, W. N. A. Bergius, L. R. Hutchings, Electrospinning superhydrophobic fibers using surface segregating end-functionalized polymer additives, Macromolecules 44 (2011) 6461–6470.
[60] S. A. Kulinich, M. Farzaneh, Effect of Contact Angle Hysteresis on Water Droplet Evaporation from Super-Hydrophobic Surfaces. Appl. Surf. Sci. 255 (2009) 4056−4060.
[61] Z. Guo, W. Liu, Sticky Superhydrophobic surface. Appl. Phys. Lett. 90 (2007) 223111-223113.
[62] L. Mahadevan, Non-stick water, Nature 411 (2001) 895-896.
[63] A. Johansson, P. Kollman, S. Rothenberg, J. McKelvey, Hydrogen bonding ability of the amide group, J. Amer. Chem. Soc. 96 (1974) 3794-3800.
[64] Y. Lai, C. Lin, J. Huang, H. Zhuang, L. Sun, T. Nguyen, Markedly controllable adhesion of superhydrophobic spongelike nanostructure TiO_2 films, Langmuir 24 (2008) 3867-3873.
[65] G. Nellis, S. Klein, Heat transfer, Cambridge University Press, UK, 2008.
[66] V. Di Tullio, N. Proietti, D. Capitani, Unilateral NMR to study water diffusion and absorption in stone-hydrogel systems, Micropor. Mesopor. Mat. (2017) https://doi.org/10.1016/j.micromeso.2017.07.011.
[67] L. L. Latour, R. L. Kleinberg, P. P. Mitra, C. H. Sotak, Pore-size distributions and tortuosity in heterogeneous porous media, J. Magn. Reson. 112 (1995) 83-91.
[68] P. B. Lorenz, Tortuosity in porous media, Nature 189 (1961) 386-387.